Microwave surface impedance of proximity-coupled Nb/Al bilayer films

Michael S. Pambianchi, S. N. Mao, and Steven M. Anlage
Center for Superconductivity Research, Department of Physics, University of Maryland, College Park, Maryland 20742-4111
(Received 16 February 1995)

The surface resistance and magnetic penetration depth in proximity-coupled superconductor/normal-metal (Nb/Al) bilayers are examined to study the electrodynamics of layered structures with spatially inhomogeneous superconducting order parameter. The effective penetration depth $\lambda_{eff}(T)$ obeys $\Delta\lambda_{eff}(T) \sim T^n$, where $n \leq 1$, at low temperatures, distinctly different from the exponential behavior of Nb. An accompanying drop in the surface resistance R_s occurs in the same temperature range. A model of the bilayer electrodynamics explicitly including the effects of proximity coupling is developed, and the behavior of both λ_{eff} and R_s is consistently described. We find that a treatment of coherence effects in the proximity-coupled normal-metal layer is necessary to properly describe the behavior of $R_s(T)$.

A superconducting system with a spatially inhomogeneous order parameter $\Psi = \Psi(x)$ may exhibit electrodynamic properties dramatically different from those of a pure superconductor, where $\Psi = \text{const}$. Several theories[1–4] of cuprate superconductivity invoke the concept of a spatially varying order parameter in the direction perpendicular to the copper-oxygen planes, and recent experiments by Müller[5] on the intrinsic Josephson effect in cuprates indicates that this is indeed reasonable. Here, we present microwave surface impedance data on proximity-coupled superconductor/normal-metal (S/N) bilayer films as a first step to better understand the electrodynamics of a layered system with a position dependent $\Psi(x)$.

Magnetization measurements,[6–8] mutual inductance measurements,[9] Josephson penetration depth measurements,[10] and resonant microwave measurements[11] on various low-T_c proximity-coupled S/N systems have shown that the magnetic screening length λ_{eff} can exhibit temperature dependences such as $\Delta\lambda_{eff}(T) \sim T$ at low temperatures. Data presented here on Nb/Al bilayer films show that both the surface resistance $R_s(T)$ and the screening length $\lambda_{eff}(T)$ can exhibit linear or sublinear T dependences as $T \rightarrow T_{cN}$, where T_{cN} is the superconducting transition temperature of the Al layer. We demonstrate that the drops in $R_s(T)$ and $\lambda_{eff}(T)$ at low temperature can both be explained by a simple model of proximity-effect electrodynamics.

The geometry of the bilayer system we consider is shown in the inset of Fig. 1. The Nb films were prepared on R-plane sapphire substrates and coated with thin Al layers, with which Nb can form clean proximity-coupled interfaces.[12] The deposition chamber was evacuated to 1×10^{-7} Torr and the Nb target presputtered to remove surface contaminants and improve oxygen gettering. Niobium was deposited at 30 Å/sec to a thickness of 1 μm by dc magnetron sputtering in 5 mTorr flowing Ar, at a substrate temperature of 110 °C. Bare Nb films had resistivity ρ_n (10 K) ≈ 1 $\mu\Omega$ cm and residual resistivity ratio ρ_n (300 K)/ρ_n(10 K) ≈ 4.

The substrate was then rotated *in situ* (without breaking vacuum) and Al was deposited at 12 Å/sec to a thickness d_N, where 100 Å $\leq d_N \leq$ 600 Å. The substrate temperature during Al sputtering was ~100 °C. The samples produced by this method had bilayer transition temperatures T_{cNS} in the range 9.0–9.1 K as determined from ac susceptibility measurements. Point-contact spectroscopy (PCS) measurements on the bilayers were performed in the manner of van Son, van Kempen, and Wyder.[13] The dynamic resistance dV/dI fit the simple Blonder-Tinkham-Klapwijk[14] form with interface boundary scattering parameter $Z < 0.2$ and attenuation factor in

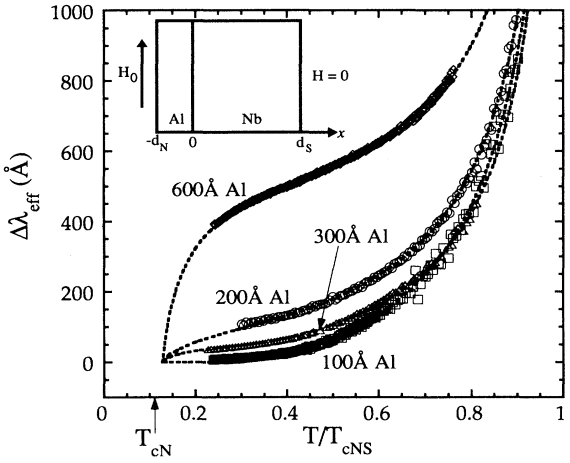

FIG. 1. Change in effective penetration length $\Delta\lambda_{eff}(t) = \lambda_{eff}(t) - \lambda_{eff}(t = 0.128)$ vs reduced temperature $t = T/T_{cNS}$ for proximity-coupled Nb/Al bilayer films with 1 μm Nb thickness and Al thicknesses 100, 200, 300, and 600 Å. Data for bare Nb sample (not shown) is nearly identical to that of the 100 Å Al sample. Dashed lines are fits to the proximity-coupled bilayer model presented in the text. Inset: bilayer geometry, with S/N interface at $x = 0$.

the normal metal $\Lambda_{PCS} \sim 0.5$, indicating good proximity coupling at the S/N interface and dirty Al. Bilayer resistivity measurements showed $\rho_n(300\text{ K})/\rho_n(10\text{ K}) \approx 4$, suggesting that $\rho_{Al} \geq 3\rho_{Nb}$.

The surface impedance of the bilayers was measured at 11.5 GHz using the parallel-plate resonator technique.[15,16] The effective penetration depth $\Delta\lambda_{eff}(T)$ and surface resistance $R_s^{eff}(T)$ were calculated using the expressions $\Delta\lambda_{eff}(T) \equiv \lambda_{eff}(T) - \lambda_{eff}(2\text{ K}) = (d/2)\{[f_0(2\text{ K})/f_0(T)]^2 - 1\}$ and $R_s^{eff}(T) = \pi\mu_0 d f_0(T)/Q(T)$,[17] where $d = 25$ μm was the thickness of the dielectric material (Teflon) separating the two plates.

The resulting $\Delta\lambda_{eff}(T)$ data for the proximity-coupled Nb/Al bilayers are shown in Fig. 1. The sample with $d_N = 100$ Å behaved much like a homogeneous, single-layer superconductor, fitting the standard $\lambda_{BCS}(T)$ temperature dependence given by Mühlschlegel.[18] The other three samples studied ($d_N = 200, 300$, and 600 Å) did not fit this dependence well, with the fit worsening as d_N increased. They displayed a noticeable region[19] where $\Delta\lambda_{eff}(T) \sim T$. When the Al layer was removed from the 300 Å Al sample by etching in NaOH, and the bare Nb film underneath measured, the BCS temperature dependence was regained. To explain the behavior of the bilayer data, a model of the electrodynamics of the entire bilayer was developed, explicitly including the effects of proximity coupling.

The model[19] first calculates the penetration profiles of the magnetic field $H(x)$ and the supercurrent density $J_s(x)$ inside a proximity-coupled S/N bilayer film. We assume a local penetration depth $\lambda_N(x,T)$ in the Al layer, inversely proportional to the spatially dependent pair potential $\Psi_N(x,T)$ induced by proximity coupling.[20] Our model, based on Ginzburg-Landau theory, requires that $\Psi_N(x,t)$ be small, and hence applies at temperatures in the vicinity of T_{cNS}. By solving Maxwell's equations with the generalized London equations as constitutive relations, and assuming the form $\lambda_N(x,T) = \lambda_N(0,T)e^{-K(T)x}$ for $x < 0$ and $\lambda_S(x,T) = \lambda_{BCS}(T)$[21] for $x > 0$, one can obtain analytical expressions for $H(x)$ and $J_s(x)$ inside the bilayer, given previously in Ref. 19.

Here, $\lambda_N(0,T)$ is the local penetration depth of the Al layer at the interface between the two metals. We postulate $\lambda_N(0,T) \sim 1/\Delta_S(T)$, where $\Delta_s(T)$ is the BCS energy gap in the Nb layer, as suggested by proximity-effect theory.[20] The parameter $K^{-1}(T)$ describes the decay length scale of $\Psi_N(x,T)$ in the Al layer in the single Matsubara frequency approximation.[22] In the dirty limit it is given by the solution to $\ln(T/T_{cN}) = \psi(\frac{1}{2}) - \psi[\frac{1}{2} - \hbar D_N K^2/(4\pi k_B T)]$, where ψ is the digamma function, $D_N = v_{FN} l_{mfp}/3$, and v_{FN} and l_{mfp} are the Fermi velocity and quasiparticle mean-free path in the Al layer, respectively. The value $T_{cN} = 1.14$ K was used for Al. The expression for $K^{-1}(T)$ appropriate for the clean limit was found to produce poor fits to the data, consistent with the PCS and resistivity results, indicating that the Al layers were in the dirty limit.

The model then calculates the inductance per unit length of a parallel-plate transmission line made up of two proximity-coupled S/N bilayer films. The total inductance is expressed in terms of an effective penetration depth $\lambda_{eff}(T)$, defined in Ref. 19. The $\Delta\lambda_{eff}(T)$ data were fit to that expression, yielding the parameter values shown in Table I. For $d_N = 100$ Å, the values of $\lambda_N(0,0)$ and $\lambda_S(0)$ are nearly the same, and K^{-1} (4.6 K) is much larger than the Al thickness. This sample thus behaved as a pure superconductor with $\lambda(0) = 700$ Å and $T_c = 9.2$ K. For the samples with $d_N = 200$ and 300 Å, the best fits occur with Nb parameters $\lambda_s(0) = 600$ Å and $T_{cNS} = 9.2$ and 9.3 K, respectively. The decay lengths are also comparable, with K^{-1} (4.6 K) = 218 and 122 Å, respectively. The values of $\lambda_N(0,0)$ were quite different, however, with $\lambda_N(0,0) = 380$ and 1390 Å, respectively. The 300 Å Al sample also had much lower surface resistance, suggesting that the underlying Nb dominated the surface impedance. This is confirmed by BCS fit[18] parameters $\lambda_S(0) = 585$ Å and $T_c = 9.0$ K for the bare Nb films after stripping off the 300 Å Al layer. The sample with 600 Å Al showed the most rapid decrease of $\Delta\lambda_{eff}$ for $T < 3$ K. The Nb parameter values were $\lambda_s(0) = 560$ Å and $T_{cNS} = 9.2$ K. The Al layer parameters were consistent with those of the other samples: $\lambda_N(0,0) = 361$ Å and K^{-1} (4.6 K) = 130 Å.

For all Al thicknesses the proximity model discussed above and in Ref. 19 fits the Nb/Al bilayer $\Delta\lambda_{eff}$ data better than when the Al is neglected and the sample treated as a bare superconductor. The parameters $\lambda_S(0)$ and T_{cNS} describing the Nb layer also agree closely for all d_N. The parameters describing the Al layer are consistent with variations in materials parameters in thin Al layers.[23] The values of $\lambda_N(0,0)$ are all greater than the London penetration depth $\lambda_L = 180$ Å for Al, suggesting that only a fraction of the available electrons are effective in screening the applied field, as expected in the dirty limit.

The effective surface resistance data[17] on Nb/Al bilayers are shown in Fig. 2. The bare Nb data fit the Mattis-Bardeen[24] temperature dependence very closely with normal-state conductivity $\sigma_{Nb} = 8.77 \times 10^7\ \Omega^{-1}\ m^{-1}$, in agreement with dc conductivity results to within experimental error. However, each bilayer sample showed a departure from pure superconducting behavior at the lowest temperatures, particularly the sample with 600 Å Al, with the drop occurring at the same temperature as the decrease in $\Delta\lambda_{eff}(T)$ shown in Fig. 1. This

TABLE I. Normal-metal layer thicknesses and fitting parameters for $\Delta\lambda_{eff}(T)$ data on Nb/Al bilayers. The results of a BCS fit to single-layer Nb ($d_N = 0$) data obtained by removing the Al from the 300 Å Al bilayer sample are also given.

d_N (Å)	λ_N (0,0) (Å)	K^{-1} (4.6 K) (Å)	$\lambda_s(0)$ (Å)	T_{cNS} (K)
0			585	9.0
100	792	1342	700	9.2
200	380	218	600	9.3
300	1390	122	600	9.2
600	361	130	560	9.2

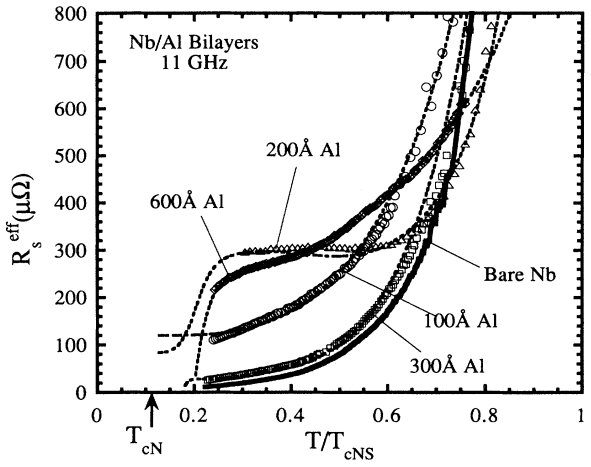

FIG. 2. Effective surface resistance measured at 11 GHz vs reduced temperature for proximity-coupled Nb/Al bilayer films with 1 μm Nb thickness and Al thicknesses 100, 200, 300, and 600 Å. Dashed lines are fits to the proximity-coupled bilayer model presented in the text. Solid line is data for a bare Nb sample.

striking similarity suggests that both $\Delta\lambda_{eff}(T)$ and $R_s^{eff}(T)$ may be described by a single electrodynamics model. The screening model of S/N bilayers given previously[19] ignored losses; now we must include losses to first order, using a treatment based on the Mattis-Bardeen theory.[24]

The model first calculates the real part of the conductivity σ_1. In the Al layer we assume $\sigma_1=\sigma_{1N}(x,T)$ due to the spatially varying pair potential $\Psi_N(x,T)$, and $\sigma_1=\sigma_{1S}(T)$, independent of x, in the Nb layer. Further, we postulate a local BCS gap $\Delta_N(x,T)$ in the excitation spectrum of the Al layer given by $\Delta_N(x,t)=[\Delta_S(T)/\alpha]e^{K(T)x}$ and a spatially constant BCS gap $\Delta_S(T)$ in the Nb layer given by the values tabulated by Mühlschlegel.[18] Finally, we calculate the local value of $\sigma_{1N}(x,T)/\sigma_N$ as a function of ω, T and $\Delta_N(x,T)$ in the Al layer using the Mattis-Bardeen theory, and the corresponding quantity $\sigma_{1S}(T)/\sigma_S$ (independent of position) in the Nb layer, where σ_N and σ_S are the bulk normal-state conductivities of Al and Nb, respectively. The Nb layer is treated as a standard BCS superconductor throughout.

The surface resistance can be expressed as $R_s=(1/H_0^2)\mathrm{Re}\int J(x)\cdot E(x)^* dx$, where $J(x)$ is the total rf current density, $E(x)$ is the electric field, and the integral is performed over the entire bilayer thickness. We calculate $J(x)=-dH/dx$ in the manner described in Ref. 19, first ignoring normal fluid contributions, and then calculate $E(x,T)$, including the losses to first order, using $J(x,T)=[\sigma_{1N}(x,T)+1/i\omega\mu_0\lambda_N^2(x,T)]E(x,T)$ for the Al layer and a similar expression in the Nb layer. We obtain the following expression for the surface resistance of the proximity-coupled bilayer:

$$R_s(T)=\frac{1}{H_0^2}\int_{-d_N}^{0}\frac{\sigma_{1N}(x,T)}{\sigma_{1N}^2(x,T)+[1/\omega\mu_0\lambda_N^2(x,T)]^2}(K(T)p^2)^2[AI_0(p)-BK_0(p)]^2dx$$
$$+\frac{1}{H_0^2\lambda_S^2(T)}\frac{\sigma_{1S}(T)}{\sigma_{1S}^2(T)+[1/\omega\mu_0\lambda_S^2(T)]^2}\left\{\frac{\lambda_S(T)C^2}{2}(e^{2d_s/\lambda_s}-1)-2CDd_s-\frac{\lambda_S(T)D^2}{2}(e^{-2d_s/\lambda_s}-1)\right\}, \quad (1)$$

where $p=p(x,T)=[K(T)\lambda_N(0,T)]^{-1}e^{K(T)x}$ and I_0 and K_0 are modified Bessel functions. The constants A, B, C, and D have units of magnetic field and are determined by satisfying appropriate magnetic boundary conditions. They are given in Ref. 19. This expression was used to fit R_s^{eff} data on Nb/Al bilayers.

The R_s fits in Fig. 2 all used the same values of $\lambda_S(0)$ and T_{cNS} that were used to fit $\Delta\lambda_{eff}(T)$ data in Fig. 1, and are described by the fitting parameters given in Table II. The model is valid for $T\geq 2$ K, but as $T\rightarrow T_{cN}$, the decay length $K^{-1}(T)$ diverges and the model no longer applies, since it requires small $\Psi(x,T)$. The fitting curves shown in Fig. 2 therefore are correct for the range of temperatures measured, but would be altered near $T=T_{cN}$. The values of $\lambda_N(0,0)$ and K^{-1} (4.6 K) producing the best fits to the R_s^{eff} data correspond closely to those describing the $\Delta\lambda_{eff}(T)$ data. Notable exceptions are $\lambda_N(0,0)$ for 300 Å Al and K^{-1} (4.6 K) for 100 Å Al. In both cases, however, the length scale in question is much larger than the Al thickness, leading to greater uncertainty in its value.

The various $R_s^{eff}(T)$ behaviors shown in Fig. 2 are due to differing values of σ_N and σ_S. Even local minima in $R_s^{eff}(T)$ are possible, as seen with the 200 Å Al sample.

TABLE II. Normal-metal layer thicknesses and fitting parameters for $R_s^{eff}(T)$ data on Nb/Al bilayers. Bare Nb data ($d_N=0$), obtained by removing the Al from the 300 Å Al sample, was fit using the Mattis-Bardeen theory. These fits used the same values of $\lambda_S(0)$ and T_{cNS} given in Table I. The parameter α was taken to be unity.

d_N (Å)	$\lambda_N(0,0)$ (Å)	K^{-1} (4.6 K) (Å)	σ_N $(\Omega\ \mathrm{m})^{-1}$	σ_S $(\Omega\ \mathrm{m})^{-1}$
0				8.77×10^7
100	700	435	1.09×10^6	4.05×10^8
200	300	154	2.66×10^9	8.14×10^7
300	600	125	3.98×10^9	2.13×10^8
600	360	240	1.00×10^9	2.62×10^7

The values of σ_N for the 200, 300, and 600 Å Al thicknesses appear larger than accepted bulk Al values, however. Also, the best fits to the temperature dependence of $R_s^{\text{eff}}(T)$ were produced with $\alpha=1.0$, smaller than the expected value $\alpha\approx N_{\text{Nb}}V_{\text{Nb}}/N_{\text{Al}}V_{\text{Al}}=2.2$,[25] where N is the density of states at the Fermi level and V is the BCS coupling constant.[22] These values of σ_N and α are associated with the assumption of a local gap $\Delta_N(x,T)$, which, though nonrigorous,[22] enables one to formulate an equivalent picture of the local excitations involved in the absorption of radiation. The magnitude and temperature dependence of the decay length $K^{-1}(T)$ can still be discerned, though the values of the fitting parameters σ_N and α producing the best fits may not be physically reasonable when $K^{-1}(T)\ll d_N$. The value $\alpha=1.0$ simply results in a larger gap $\Delta_N(x,T)$, decreasing the quasiparticle population and requiring artificially large values of σ_N to compensate.

The Mattis-Bardeen-based model also provides a way to include coherence effects[26] between excitations in the Al layer, a phenomenon which is detectable by electromagnetic absorption and nuclear magnetic resonance, but few other methods. To our knowledge, the only other evidence of case-II coherence effects in a proximity-coupled normal metal was seen by Zheng *et al.*[27] in the nuclear-spin-lattice relaxation rate $1/T_1$ of ^{63}Cu nuclei in proximity-coupled Nb/Cu multilayers. The successful inclusion of coherence effects in our model further strengthens the notion that the proximity-induced state in a normal metal resembles a true superconducting state, even in the properties of its excitation spectrum. Such effects are not present in a simple two-fluid model, which we found to be inadequate in describing the temperature dependence of $R_s^{\text{eff}}(T)$.

We have introduced a compelling description of the electrodynamics of proximity-coupled bilayers which reproduces the temperature dependence of $R_s^{\text{eff}}(T)$ and $\Delta\lambda_{\text{eff}}(T)$ at low T in Nb/Al bilayers. The model presented here represents an important step in understanding the electrodynamic response of layered systems where proximity coupling between the layers may be active. Further work is required to explore the relevance of these effects to the electrodynamic behavior of cuprate superconductors.

The authors acknowledge G. Deutscher, J. Claassen, S. Wolf, V. Kresin, and C. J. Lobb for their helpful comments and A. Das for assistance with PCS measurements and thin-film deposition. This work was supported by Grant No. NSF-DMR-9123198.

[1]T. Koyama, N. Takezawa, Y. Naruse, and M. Tachiki, Physica C **194**, 20 (1992).
[2]A. I. Buzdin, V. P. Damjanovic, and A. Yu. Simonov, Physica C **194**, 109 (1992).
[3]R. A. Klemm and S. H. Liu, Phys. Rev. Lett. **74**, 2343 (1995).
[4]V. Z. Kresin and S. A. Wolf, Phys. Rev. B **46**, 6458 (1992).
[5]R. Kleiner and P. Müller, Phys. Rev. B **49**, 1327 (1994); P. Müller, *Proceedings of the Solid State Division,* Physikalische Gesellschaft Spring 1994 Meeting, Münster (Friedrich Vieweg und Sohn VmbH, Wiesbaden, 1994).
[6]Y. Oda, A. Sumiyama, and H. Nagano, Jpn. J. Appl. Phys. **22**, 464 (1983).
[7]A.C. Mota, in *Josephson Effect-Achievements and Trends,* edited by A. Barone (World Scientific, Singapore, 1986), p. 248.
[8]K. Kanoda, H. Mazaki, N. Hosoito, and T. Shinjo, Phys. Rev. B **35**, 8413 (1987).
[9]J. H. Claassen, J. E. Evetts, R.E. Somekh, and Z. H. Barber, Phys. Rev. B **44**, 9605 (1991).
[10]R. W. Simon and P. M. Chaikin, Phys. Rev. B **23**, 4463 (1981); R. W. Simon and P. M. Chaikin, Phys. Rev. B **30**, 3750 (1984).
[11]J. R. Hook and J. A. Battilana, J. Phys. F **6**, 1689 (1976); J. R. Hook, J. Low Temp. Phys. **23**, 645 (1976).
[12]T. Imamura and S. Hasuo, IEEE Trans. Magn. **27**, 3172 (1991).
[13]P. C. van Son, H. van Kempen, and P. Wyder, Phys. Rev. Lett. **59**, 2226 (1987).
[14]G. E. Blonder, M. Tinkham, and T. M. Klapwijk, Phys. Rev. B **25**, 4515 (1982).
[15]R. C. Taber, Rev. Sci. Instrum. **61**, 2200 (1990).
[16]M. S. Pambianchi, S. M. Anlage, E. S. Hellman, E. H. Hartford, Jr., M. Bruns, and S. Y. Lee, Appl. Phys. Lett. **64**, 244 (1994).
[17]The full expression relating the measured Q and R_s is $1/Q=R_s^{\text{eff}}/\pi\mu_0 f_0 d=(1/Q_{\text{rad}})+(1/Q_{\text{coup}})+\tan\delta+(R_s/\pi\mu_0 f_0 d)$. The three extrinsic sources of loss (radiation, coupling loss, and dielectric loss) amounted to less than 20 $\mu\Omega$ in all cases presented in this paper. See Ref. 15.
[18]B. Mühlschlegel, Z. Phys. **155**, 313 (1959).
[19]M. S. Pambianchi, J. Mao, and S. M. Anlage, Phys. Rev. B **50**, 13 659 (1994).
[20]G. Deutscher, J. P. Hurault, and P. A. van Dalen, J. Phys. Chem. Solids **30**, 509 (1969). As discussed in Ref. 19, we omit the explicit factor of $T^{1/2}$ in Deutscher's expression for $\lambda_N(0,T)$, however, because it is unphysical as $T\to 0$. We employ the model described as Model I_A in Ref. 19.
[21]In Ref. 19 we found the depression of $\Psi(x)$ in the Nb layer near the S/N interface has a negligible effect on the screening of magnetic field except near T_{cNS}, so we simply assume $\lambda_s=$const across the Nb layer. See P. G. de Gennes, *Superconductivity of Metals and Alloys* (Addison-Wesley, New York, 1966), p. 233.
[22]P. G. de Gennes, Rev. Mod. Phys. **36**, 225 (1964).
[23]J. Kwo, K. Wertheim, M. Gurvitch, and D. N. E. Buchanan, Appl. Phys. Lett. **40**, 675 (1982).
[24]D. C. Mattis and J. Bardeen, Phys. Rev. **111**, 412 (1958).
[25]E. L. Wolf, *Principles of Electron Tunneling Spectroscopy* (Oxford University Press, New York, 1985), p. 524–527.
[26]M. Tinkham, *Introduction to Superconductivity* (McGraw-Hill, New York, 1975), p. 57.
[27]G. Zheng, Y. Kohori, Y. Oda, K. Asayama, R. Aoki, Y. Obi, and H. Fujimori, J. Phys. Soc. Jpn. **58**, 39 (1989).